



The impact of secondary inorganic aerosol emissions change on surface air temperature in the Northern Hemisphere

Chunjiang Zhou^{1,3} · Peng Liu⁴ · Gang Huang^{1,2,3} · Jintai Lin⁴ · Kaiming Hu^{1,5} · Lulu Chen⁴ · Jingxu Wang⁴ · Sixuan Li^{1,3} · Su Wang^{1,3} · Ruijing Ni⁴

Received: 2 March 2020 / Accepted: 27 April 2020 / Published online: 15 May 2020
© Springer-Verlag GmbH Austria, part of Springer Nature 2020

Abstract

Using the Community Earth System Model (CESM) version 1.2, this study investigates the changes in secondary inorganic aerosols (SIOAs) over the Northern Hemisphere from 1850 to 2007, regional contributions, and consequences on surface air temperature. Results show that SIOAs changes can be divided into two stages. At the first stage (1850–1980), European and North American SIOAs concentrations increase, with a cooling effect especially over Europe and Eastern Siberia. At the second stage (1980–2007), SIOAs concentrations over Europe and North America are reduced with a warming effect in the mid-high latitudes, whereas SIOAs increase over East Asia and South Asia leading to a cooling effect there. The temperature changes over the emission source regions are mainly driven by radiative forcing. Horizontal transfer of heat leads to a temperature response in the Siberian region.

1 Introduction

Aerosols generated by human activities not only pollute the air, but also affect Earth's radiation budget. By scattering and absorbing solar radiant energy, aerosols change radiant flux at top, bottom, and inside of the atmospheric column (Ramanathan and Feng 2009). Secondary aerosols are produced by chemical reactions of gaseous and particulate pollutants discharged by humans into atmosphere (mainly photochemical reactions caused by ultraviolet light, ozone, and OH

radicals) (Volkamer et al. 2006). Secondary inorganic aerosols (SIOAs) mainly include sulfate, nitrate, and ammonium. The main component is sulfate. The direct reducing-temperature effect of SIOAs is opposite to the radiation effect of greenhouse gases by directly reflecting solar short-wave radiation and reducing the amount of radiation reaching ground (Lin et al. 2016). Although understanding of aerosols and their climate impacts have improved dramatically, aerosol radiative forcing as well as the effects on the surface temperature results is still a big uncertainty in climate research (Boucher and Randall 2013). As reported by Myhre et al. (Myhre et al. 2013), the total radiative forcing of aerosols (including aerosol-cloud interactions) in 2011 relative to 1750 is in the range (-1.9 to -0.1) W m^{-2} . Most of its uncertainty is buried in the interaction between clouds and aerosols (He et al. 2015). Moreover, the regional response of atmospheric circulation to global and regional anthropogenic aerosol forcing is not yet well understood and constrained (Xie et al. 2013). To improve future climate projections, a deep understanding of the temperature response to scattering anthropogenic aerosols is needed.

The emissions of SIOAs precursors are mainly from ore combustion, which is closely related to industrial development. With the development of industry and economy, there is a large regional difference in SIOAs precursors emissions in the Northern Hemisphere since the industrial revolution (Smith et al. 2011; Tsigaridis et al. 2006). Global emissions

✉ Gang Huang
hg@mail.iap.ac.cn

¹ State Key Laboratory of Numerical Modeling for Atmospheric Sciences and Geophysical Fluid Dynamics (LASG), Institute of Atmospheric Physics, Chinese Academy of Sciences, Beijing 100029, China
² Laboratory for Regional Oceanography and Numerical Modeling, Qingdao National Laboratory for Marine Science and Technology, Qingdao 266237, China
³ University of Chinese Academy of Sciences, Beijing 100049, China
⁴ Laboratory for Climate and Ocean-Atmosphere Studies, Department of Atmospheric and Oceanic Sciences, School of Physics, Peking University, Beijing 100871, China
⁵ Center for Monsoon System Research, Institute of Atmospheric Physics, Chinese Academy of Sciences, Beijing 100029, China

reach the peaking in the 1970s, with a significant decrease over the 1990s, and likely increasing slightly in recent years (Smith et al. 2011). The emissions of SIOAs precursors in developed and developing countries have different trends. For example, the US Clean Air Act of 1970 limits fixed (industrial) and mobile device emissions to address pollutant emissions and health issues (Aas et al. 2019). Such regulations have guaranteed significant reductions in SO₂ emissions in the USA and Europe in the late twentieth century (Hoesly et al. 2018). Meanwhile, more than doubled energy consumption in Asia between 1980 and 2003, caused a rapid growth in Asian emissions, by 119% for SO₂, and 176% for NO_x (Lu et al. 2010; Ohara et al. 2007). Emissions in China are estimated to have peaked about 2006, and then declined. SO₂ emissions from India continue to increase sharply (Klimont et al. 2013). The few studies have focused on the impact of specific regional aerosol emissions on the climate in local areas (Acosta Navarro et al. 2016; Kasoar et al. 2016; Conley et al. 2018). However, the impact of such a dramatic change in the spatial distribution of SIOAs concentrations on the global climate system is limited.

Previous studies have done a lot of researches on the influence of aerosol on climate. Wang et al. (2015) find that the increasing Asian pollution accounts for the weakening of the tropics circulation, while the decreasing pollution in Europe and the USA tends to shift the circulation systems southward. In direct atmospheric response, aerosol affects precipitation and atmospheric circulation by changing radiation and cloud physics (Bollasina et al. 2013). Many studies have also focused on the influence of aerosols on circulation at regional and local scales, especially in the densely populated Asian monsoon region (Lau and Kim 2017; Li et al. 2015, 2018). Aerosols weaken the South Asian monsoon and the East Asian monsoon. However, most of these studies are limited to a certain region, such as East Asia, or focus on a certain season. There is a lack of discussion of atmospheric circulation on a large scale. Moreover, there is a lack of analysis on the influence of aerosol on climate from the perspective of long-term historical evolution.

In this article, we mainly analyze the spatial distribution changes of SIOAs concentration in the northern hemisphere, and study the impact of this change on the surface temperature in the northern hemisphere. Three nodes are selected in the year 1850, 1980, and 2007 represent before the industrial revolution, the highest period of global pollution emissions and now, respectively. The organization of sections is as follows. Section 2 introduces the model and experimental design. Section 3 analyzes the simulation results from three aspects: SIOAs concentration changes, temperature changes in the emission source area, and temperature response in other areas. Section 4 summarizes the conclusion.

2 Experiment description and analysis method

2.1 CESM1.2

The model used in this study is the atmospheric component of the Community Earth System Model (CESM) version 1.2, Community Atmospheric Model version 5.2 (CAM5.2), developed by the National Center for Atmospheric Research (NCAR) (Neale et al. 2012). CESM can simulate the entire earth system by coupling eight components, including the atmosphere, ocean, land, and sea ice. As one of the outstanding models in the Intergovernmental Panel on Climate Change (IPCC) Fifth Assessment Report (AR5), it has been used to simulate climate change (Knutti et al. 2013). CESM-CAM has advanced chemistry/aerosol treatment, and the distribution of aerosols can be simulated relatively accurately (Liu et al. 2012). Several studies have demonstrated the capability of CAM-chem to represent tropospheric and stratospheric conditions, and the influence of aerosol on local and global climate (Gantt et al. 2014; He et al. 2015; Undorf et al. 2018; Xie et al. 2016).

The chemical mechanism in this experiment is based on Model for Ozone and Related Chemical Tracers (MOZART), version 4 mechanism for troposphere (Emmons et al. 2010), with further updates (Lamarque et al. 2012). In the chemistry module used in this work, aerosol size distributions are characterized into three lognormal modes: Aitken, accumulation, and coarse modes. Aerosol species are assumed to be internally mixed within each mode and externally mixed among different modes. Both aerosol mass and particle number can be prognostic, aerosol species mainly include sulfate, dust, black carbon, and primary and secondary organic aerosol. As for the main component in SIOAs, sulfates mass is proposed as a component in each of the three aerosol modes, and most of the sulfate (~90%) is in accumulation mode (Liu et al. 2012). Sulfate is produced via H₂SO₄ condensation on existing aerosols, whereas H₂SO₄ is formed by the oxidation of SO₂. Nitrate does not contribute to aerosols. Both direct and indirect radiative effects of aerosols are included and aerosol-cloud interactions can influence both cloud droplet number and mass concentrations (Kasoar et al. 2016).

In this study, CESM1.2-CAM5 runs with a finite-volume dynamical core, with a horizontal resolution of 1.9° at latitude and 2.5° at longitude. In the vertical, there are 30 levels and the model top at approximately 40 km. Atmospheric Model Intercomparison Project (AMIP) (W. Lawrence Gates et al. 1999) experiments are performed with prescribed climatological sea surface temperature (SST) and sea ice distribution, to understand seasonal variation of anthropogenic aerosol direct and indirect effects. Dry deposition of gases and aerosols is implemented in the Community Land Model (CLM) (Oleson et al. 2004) as described in Lamarque et al. (Lamarque et al. 2011).

2.2 Experimental setup

Four cases are simulated with prescribed SST and sea ice distribution in 2000. Each case run 50 years, and the last 45 years of simulated data are used. There are one control run and three sensitivity runs. Those runs are different only in SIOAs precursor gases emissions, while the other forcing such as greenhouse gases conditions are kept at their present-day (year 2000) values, which follows the year-2000 ACCMIP emission inventory (Lamarque et al. 2010). The control experiment is performed with 1850 SIOAs precursor gases emissions, while in adjustment experiments, SIOAs precursor gases emissions are in year 1980 and 2007, the last adjustment experiment remove all anthropogenic SIOAs precursor gases emissions. Anthropogenic aerosol and precursor gases emissions are from the Community Emissions Data System (CEDS) (Hoesly et al. 2018). The difference between control and adjustment cases represents atmospheric response to SIOAs concentration changes in different regions after the industrial revolution, which are caused by industry developing (Table 1).

2.3 Temperature change analysis

$$\frac{\partial T}{\partial t} = -\vec{V} \cdot \nabla T - w(\gamma_d - \gamma) + \frac{1}{C_p} \frac{dQ}{dt}$$

The atmospheric thermodynamic equation gives a relationship between system state change and heat exchange. Dynamic process and thermodynamic process of atmosphere are interrelated and mutually constrained. The above formula is the first-order simplification of the atmospheric thermodynamic energy equation. γ_d is the dry adiabatic lapse rate, γ is the environmental lapse rate, and C_p is the specific heat at constant pressure. The left side of the equation is the local variation of temperature, which represents changes in local temperature over time. The first item on the right side of the equation is the transfer of heat from the horizontal motion of the atmosphere. The second item on the right side is temperature change caused by the vertical movement of atmosphere which is related to the stability of the atmosphere. The third item on the right side is the non-adiabatic heating term. Solar

radiation is the main form of heating atmosphere. Temperature transient response of other regions is mainly caused by advection and vertical motion of the atmosphere. Adjustment of atmospheric circulation causes heat to be transported in horizontal and vertical directions, affecting temperature. In local temperature changes, the degree of influence of different factors is not equal. The following will discuss in detail the dominant factors of local temperature changes in different situations.

3 Results

3.1 Global SIOAs concentration changes

As shown in Fig. 1, SIOAs surface concentration changes mainly distribute in three main areas: North America, Western Europe, and East Asia. These three regions are home to the largest economy of the world, with a population of more than one-third of the total population. The first phase is from 1850 to 1980 during which SIOAs concentrations in the Northern Hemisphere increases generally, with the most significant increase in Europe and North America. The SIOAs increasing over Europe (average $41.6 \mu\text{g}/\text{m}^3$) is greater than North America (average $17.40 \mu\text{g}/\text{m}^3$). SIOAs concentrations in eastern China increase by an average of $4.5 \mu\text{g}/\text{m}^3$. According to predecessors, global aerosol emissions, in particular sulfate aerosol precursor sulfur dioxide (SO_2), are dominated by sources area in North America and Europe for most of the twentieth century (Hoesly et al. 2018; Lamarque et al. 2010). Developed regions such as Europe and the USA have begun to reduce domestic pollutant emissions since the 1980s, while pollutant emissions have increased in developing regions with the development of industrialization.

Specifically, compared with 1980, SIOAs concentrations in Europe decrease by $33.36 \mu\text{g}/\text{m}^3$ on average in 2007. The reduction of extremum lies in Belarus and Ukraine. Overall, except for East Asia, South Asia, and Southeast Asia, Eurasia show a reducing trend in SIOAs. Even the northern part of Africa is affected to some extent, showing a decrease in SIOAs concentrations. Unlike in Europe, there is no significant extreme value for changes in SIOAs concentrations in North America. SIOAs concentrations reduction in North America is $5.09 \mu\text{g}/\text{m}^3$ on average with decreases relatively

Table 1 SIOAs precursor emissions disturbance in experiments

Name	SIOAs precursor gases emission year	Emission perturbation
Ctl	1850	9 Tg year^{-1}
G1980	1980	$240.5 \text{ Tg year}^{-1}$
G2007	2007	277 Tg year^{-1}
Remove	SIOAs precursor gases emissions are removed	0 Tg year^{-1}

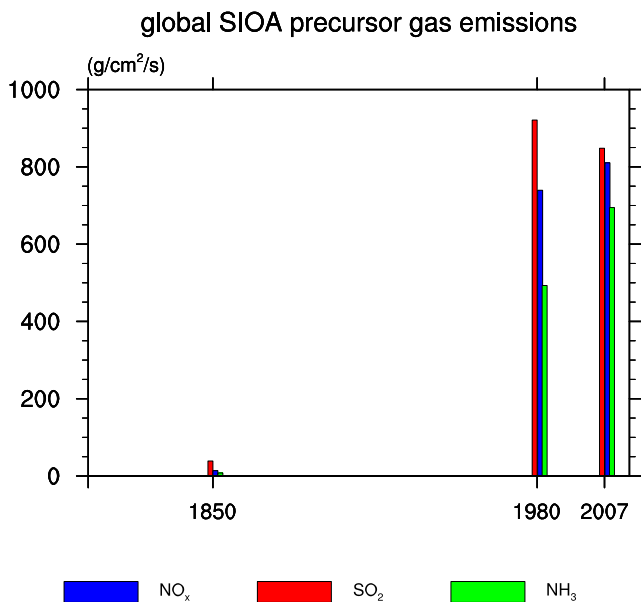


Fig 1 Perturbation of the unit grid emissions of SIOAs precursors in the model in different experiments

larger in the central US than the eastern coast. From 2007 to 1980, East Asia and South Asia show a significant increase in SIOAs concentrations. The high-value area mainly locate in

the Shandong Peninsula, adjacent parts of North China and Sichuan Basin, with a value of $18.55 \mu\text{g}/\text{m}^3$. Average SIOAs concentrations in China and India increase by $11.35 \mu\text{g}/\text{m}^3$ and $9.49 \mu\text{g}/\text{m}^3$, respectively. Concentrations of SIOAs also increase in Thailand, Myanmar, Singapore, and other regions.

Unlike greenhouse gases with a long life span and a wide distribution range, SIOAs have a life cycle of only one week. Lifetimes of sulfate in the CAM model is 3.9 days (Tilmes et al. 2015). Therefore, the distribution of SIOAs has strong local differences, and concentration is the strongest in the source emission area, decreasing to the periphery. This is related to human production and life behavior and is also affected by atmospheric circulation and meteorological conditions. These factors affect SIOAs life cycle, diffusion range, and settling velocity.

Aerosol optical thickness (AOT) or aerosol optical depth (AOD), defined as integral of the extinction coefficient of the medium in a vertical direction, can describe the effect of aerosols on light reduction (Bäumer et al. 2008). Generally, high AOD value indicates an increase in longitudinal accumulation of aerosols, thus resulting in a decrease in atmospheric visibility. Several aerosols, especially sulfate in the SIOAs component, can affect AOD (Conley et al. 2018). Therefore, it can be seen from simulation results that during two stages, AOD

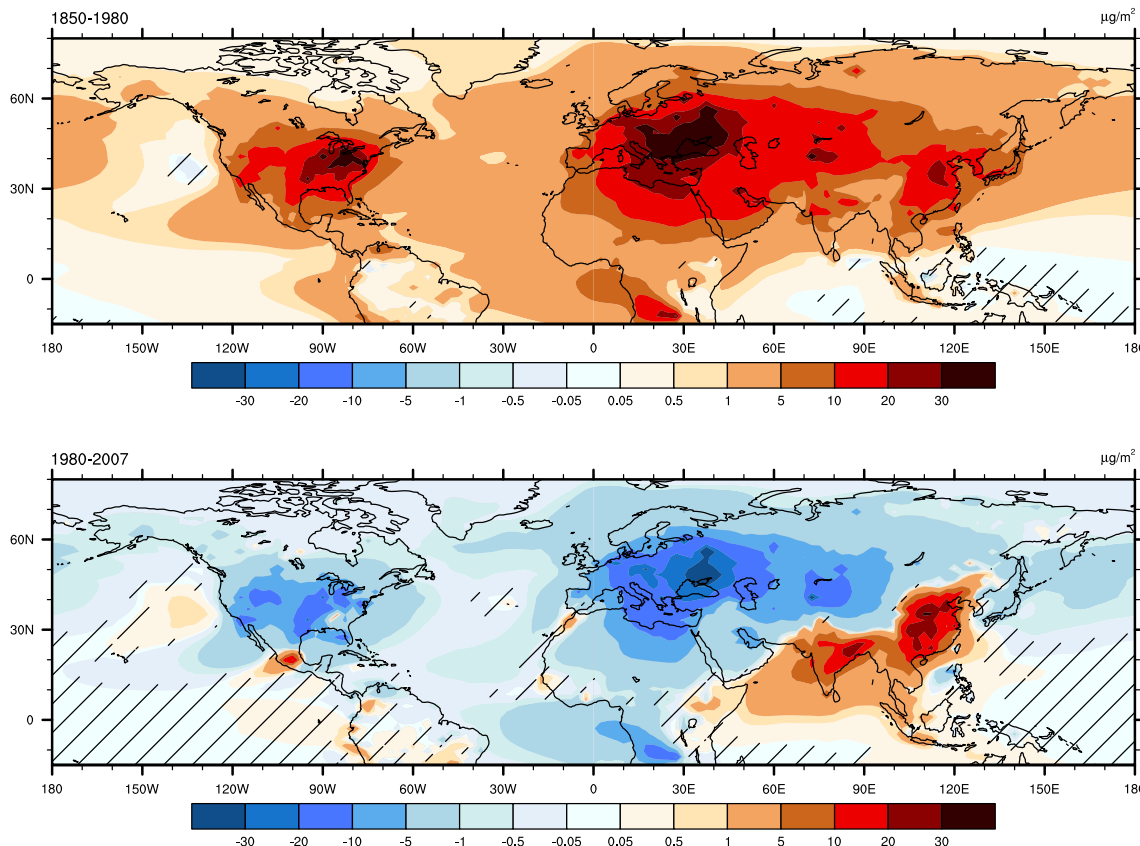


Fig. 2 Variation of surface concentrations distribution of SIOAs, 1850–1980 year and 1980–2007 year. The shading indicates that the 95% two-tailed student *t* test is not passed

also changes similarly after SIOAs concentrations disturbance. Spatial distribution of AOD value change and extreme value center are consistent with SIOAs concentrations change. The AOD in the Northern Hemisphere shows a consistent growth trend from 1850 to 1980. The most significant increase was in Europe (0.09 on average), followed by North America (0.03 on average). Over East Asia, increasing occurs only in eastern China (0.01 on average). On the global scale, AOD grows by an average of 0.11. In the second phase, AOD reduction is concentrated in Europe and North America, and the extent of AOD reduction in Europe (maximum 0.17) was much greater than in North America (maximum 0.05). There are obvious high-value areas in East Asia and South Asia, located in central China (0.08 on average) and northeastern India (0.03 on average) respectively. In terms of seasonal changes, it also shows a stable consistency with variation of SIOAs concentrations. The results show that AOD responses are strongest in regions near to and downwind from the region of decreased/increase SIOAs emissions (Figure 2).

3.2 Temperature response in aerosol source areas

As mentioned in 2.3, local temperature changes are determined by different impact factors. So, the response of surface

temperature to the change of SIOAs concentrations distribution is different between the aerosol source area and the distant area. In the aerosol source area, the trend of temperature change is opposite to that of SIOAs emissions. Figure 3 shows the annual mean surface air temperature change. From 1850 to 1980, most of the Northern Hemisphere is dominated by cooling, with extreme cooling in Europe and high latitudes of Eastern Siberia, reaching -0.87 K and -0.57 K respectively. There is warming in the plains of Western Siberia and high latitudes of the plains of Eastern Europe. The same applies to the Qinghai-Tibet Plateau. From 1980 to 2007, surface temperature increases in Europe and North America where SIOAs concentrations decrease. Warming in Europe (0.13 K) is greater than North America (0.035 K), and the location of maximum warming in Europe (0.21 K) is consistent with the position of maximum SIOAs emissions reduction. In central and eastern China, India, Myanmar, and other Southeast Asian regions, SIOAs increasing, so the temperature in these places is reduced. The average temperature drop in central and eastern China can reach 0.12 K. The temperature in the Indian region decreases 0.083 K on average. Uncertainty analysis has not been performed for temperature due to lack of the necessary unforced simulation output for the version of the model used here (Conley et al. 2018; Kasoar et al. 2016).

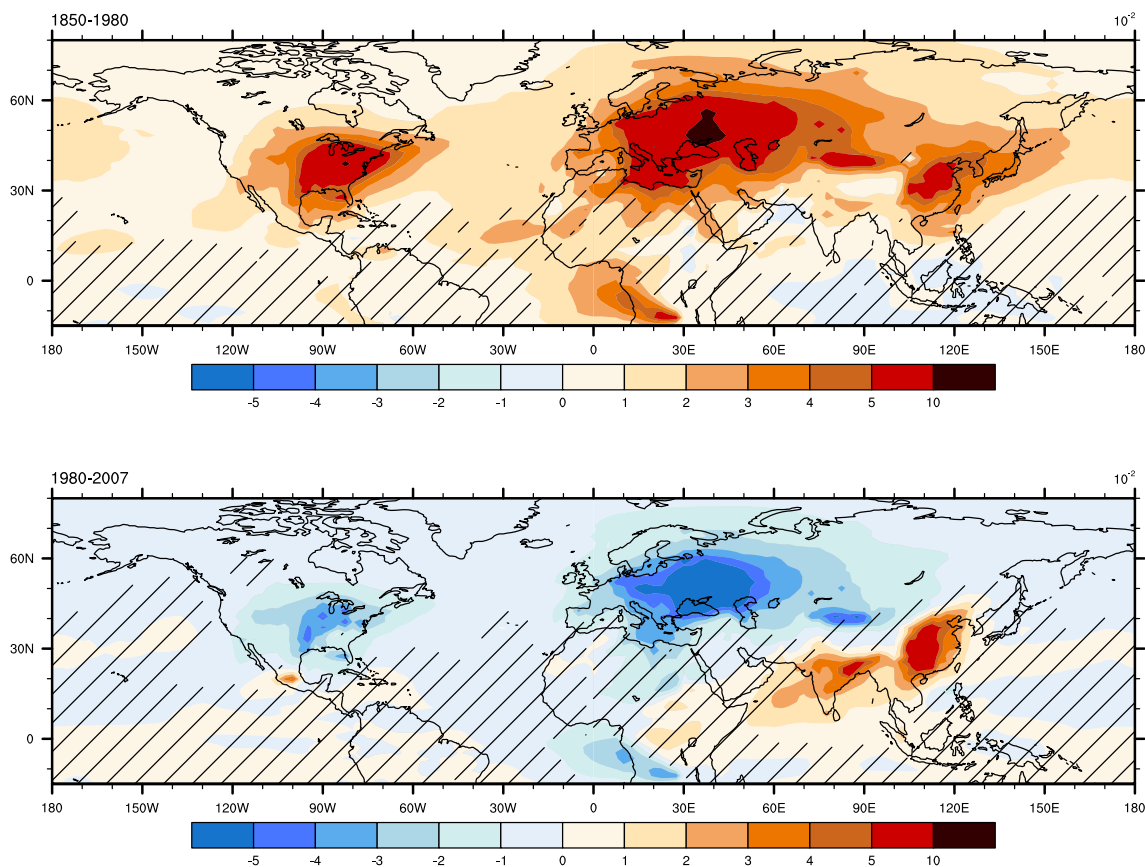


Fig. 3 Changes in aerosol optical depth in the Northern Hemisphere from 1850 to 1980, 1980 to 2007. The shading indicates that the 95% two-tailed student *t* test is not passed

In aerosol emission sources, non-adiabatic heating is dominant on local temperature change. ERF is defined as a change in net flux (SW + LW) between control and disturbance simulations using specified SST (Conley et al. 2018). Compared to transient radiative forcing, ERF is a better indicator of long-term climate forcing because it includes full adjustment of atmosphere and land models, aerosol responses from changes in emissions, transport, and deposition are taken into account in the calculations. Compared with 1850 (Fig. 4), SIOAs concentrations increasing in Europe during 1980, reduces surface solar radiant flux obtained in high latitudes of the Eurasian continent and Arctic regions. ERF in Europe decreases by an average of 4.72 W/m^2 , and the maximum reduction reached 13.12 W/m^2 . ERF in North America is also generally reduced 6.03 W/m^2 on average. There is a slight ERF decrease in East Asia and an increase in the Qinghai-Tibet Plateau. From 1980 to 2007, radiative forcing increases in Europe and the Americas, and decreases in central and eastern China, India and other Southeast Asian regions. The amount of surface radiation flux changes more than the top of atmosphere. Especially in Eastern Europe, there is a significant maximum change in surface net radiation, with a value of 5.99 W/m^2 . In central and eastern China, as well as in South and Southeast

Asia, climatic systems are more complicated due to monsoon and subtropical highs. Therefore, solar radiation changes caused by SIOAs in eastern China are not so obvious. There is a very significant reduction in solar radiation in the eastern part of the Indian Peninsula and China Tibet Junction, reaching 13.24 W/m^2 .

In addition, changes in cloud cover can also explain the differences in surface ERF to some extent. As shown in Fig. 5, in the stage between 1580 and 1980, total cloud cover increases in mid-high latitudes of the Northern Hemisphere. Areas with increased cloud cover in Eurasia are consistent with areas where surface ERF reduce. From 1980 to 2007, cloud cover has a slight decline in Europe and North America. In central and eastern China, India, and other South Asian regions, an increase in cloud cover is very obvious.

3.3 Remote response to temperature in other parts of the Northern Hemisphere

It can be seen in Fig. 3 from 1850 to 1980, SIOAs concentrations in Eastern Siberia do not change much, but temperature response is very obvious. In the stage from 1980 to 2007,

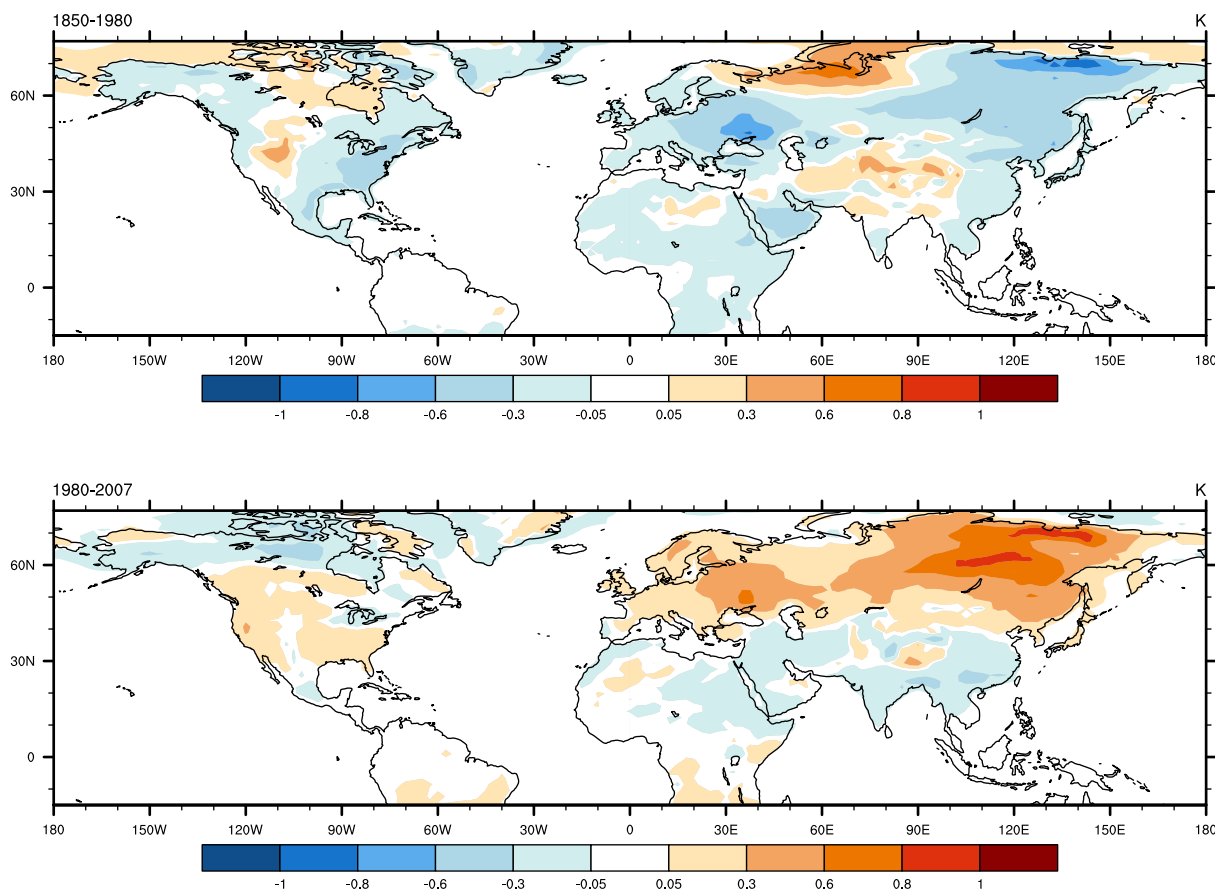


Fig. 4 Temperature response of the Northern Hemisphere after global SIOAs concentrations change from 1850 to 1980, 1980 to 2007. Significance is not evaluated as 50-year control runs are not available to assess internal variability for this model

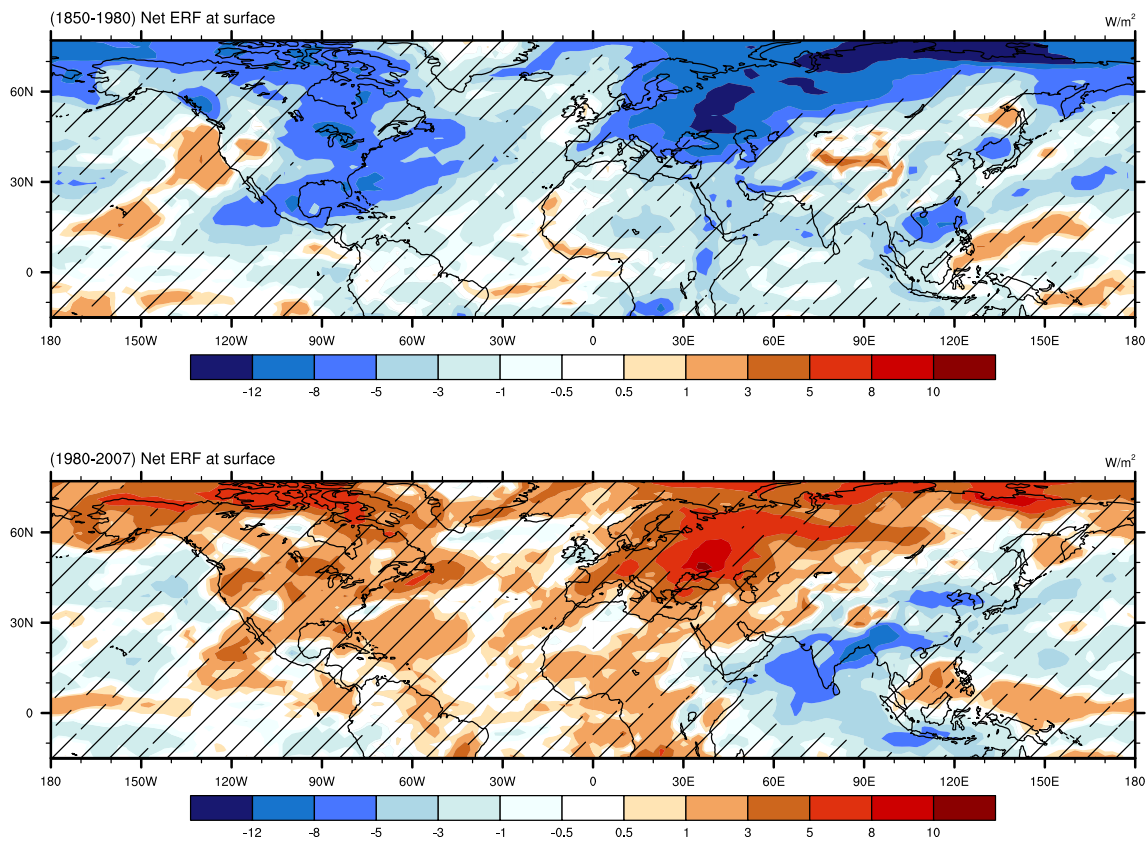


Fig. 5 Net radiation (SW + LW) changes at top of atmosphere. The shading indicates that the 90% two-tailed student *t* test is not passed

conspicuous warming is found over high latitude in the Northern Hemisphere. Average temperature rises 0.55 K. Warming also occurs in northern regions of China, such as Inner Mongolia and Xinjiang. Compared with the change in SIOAs concentrations, the temperature change in these areas is too obvious (Fig. 1). Therefore, SIOAs direct and indirect climate effects discussed in Section 3.2 are not the main reasons for temperature changes in these areas.

From temperature change of the whole atmosphere in the Northern Hemisphere, it can be found that atmospheric warming in mid-high latitudes mainly occurs at the bottom of the atmosphere. From 1850 to 1980, the surface temperature in mid-high latitudes of the Northern Hemisphere declines (Fig. 6a), while in 1980–2007, it shows significant warming (Fig. 6b). When surface temperature decreases in the Northern Hemisphere, heat transfer near the ground is characterized by negative heat transfer from low latitude to mid-high latitude (Fig. 6c). Conversely, when there is a very significant positive heat transfer in low latitude to high latitudes (Fig. 6d), surface temperature increases in mid-high latitudes of the Northern Hemisphere. The strongest heat transfer change can be seen from 50 to 70°N, which is basically consistent with the latitude of radiation changes in Europe and North America (Fig. 4). From 1850 to 1980, there are cold advection and warm advection in Eastern Siberia and Western Siberia regions, so those two regions show strong cooling and

warming respectively. From 1980 to 2007, average meridional heat transfer in Siberia (50–70° N, 60–150° E) can reach 1.52 W/m². Therefore, significant warming in the Siberian region is mainly due to warm advection that transports heat from low latitudes (Europe and northeast China). The weak cooling in the vicinity of Saudi Arabia and Iran is due to cold temperature advection from the north. In fact, cold advection from polar regions also affects Europe and North America, causing cooling in those regions. However, as the two regions are more affected by the increase in radiative forcing due to reduction in SIOAs emission concentrations, the final temperature is characterized by warming.

Air compression warming and expansion cooling caused by vertical movement of atmosphere can also affect local temperature to some extent. However, in this experiment, vertical motion can only enhance or weaken local temperature trends. It is not possible to determine or completely change the local temperature trends like a non-adiabatic heating term or a temperature advection term. For example, in the second stage, in Europe the sinking air induced adiabatic compression warming offsets partly the cooling effect of cold advection. In Siberia, the sinking induced warming effect in the region of 90–135° E is superimposed on warm advection, making warming very obvious.

The advection and vertical motion of the atmosphere are determined by circulation, which is driven by solar radiation. Following is an analysis of atmospheric circulation in the

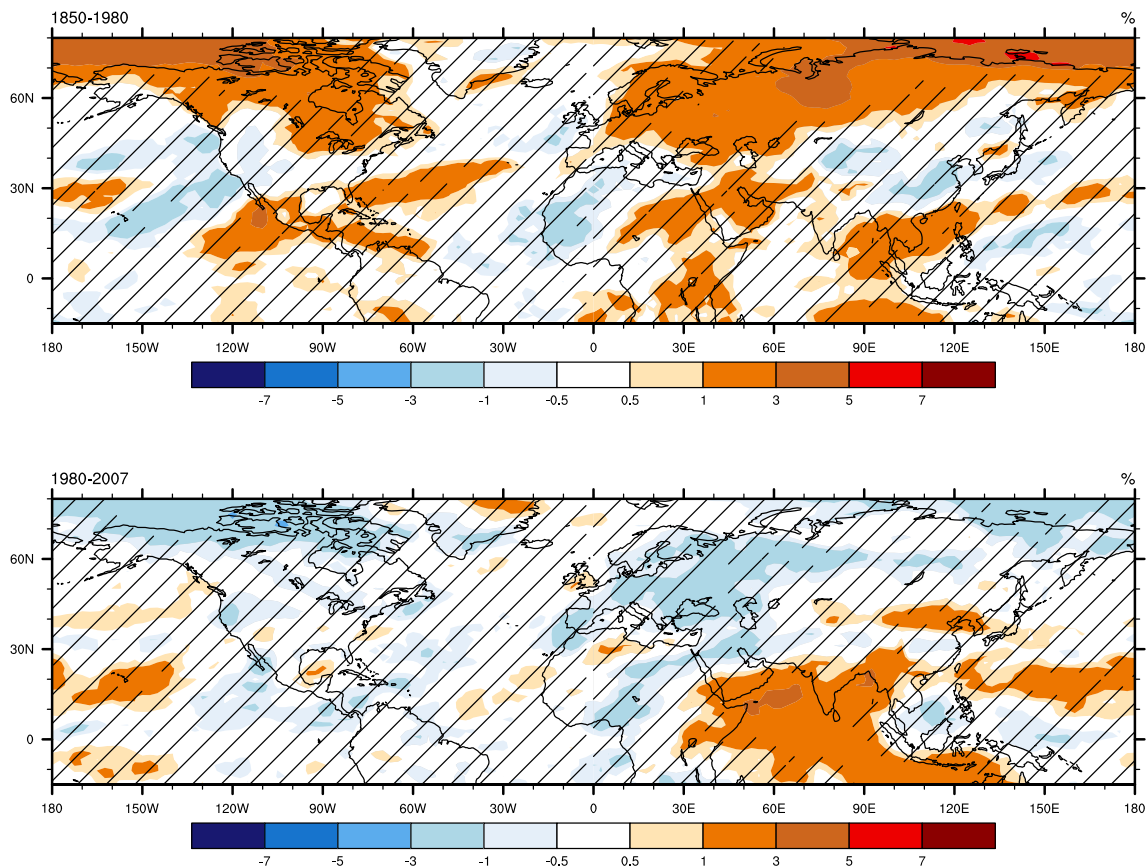


Fig. 6 Total cloud amount change. The shading indicates that the 95% two-tailed student *t* test is not passed

Northern Hemisphere to answer transient response of temperature. The effect of energy transport on atmospheric circulation is explained from the perspective of energy imbalance of the atmosphere-land model. The principle of influence of atmospheric circulation changes on temperature advection in two stages is consistent, and change of atmospheric circulation in the second stage is more complicated. Therefore, the second stage is selected as a representative for analysis (Figure 7).

Figure 8 a shows a low-level circulation. From the year 1980 to 2007, there is a significant southerly wind enhancement in the Siberian region (50–70° N, 60–150° E). They are southwesterly winds from Europe and southeasterly wind from southeast China. They carry warm air from Europe and northeast China to Siberia. There are two high pressures in the Northern Hemisphere (Fig. 8b), located in the North Pacific and North Atlantic. A low pressure lies near the Barents Sea and Siberia is located on the southeast side of polar depression, which is beneficial to southwesterly winds from Europe. It is also located on the northwest side of ground high pressure, where the southeasterly wind is prevalent. After SIOAs concentrations changed, the intensity of the ground high pressure system and the low pressure system increases. The cooling and heating effects of aerosol radiation in the mid-high latitudes of the Northern Hemisphere (40–60 N) have led to the development of 500 hPa atmospheric troughs and

ridges. Warming in Europe has led to the strengthening of the upper trough (Fig. 8c). Troughs near East Asia weakened, ridges developed, and surface pressure from East Asia to the North Pacific increased. The anticyclonic vorticity increases and converges under the action of the geostrophic deflection force, thus pressurizing the ground, and diverges under the action of the pressure gradient force in the positive transformation zone (Fig. 8b). Siberia is located in the middle of two high pressures. The air cyclone is abnormally strengthened and the central air pressure is reduced. The development of ground pressure system stabilizes low-altitude wind direction and increases wind speed, bringing warm air from low latitudes to the Siberian region, and blowing polar cold air to Europe.

In the actual Earth system, ocean plays a much larger role in heat storage and transportation than atmosphere. Response and adjustment of atmosphere to thermal imbalances are more rapid than the process of releasing heat from ocean. It is shown that ocean sends more heat to the North Pole and the warmed Arctic after the reduction of sulfur dioxide in Europe (Acosta Navarro et al. 2016). Some recent studies have shown that global warming is driven by Earth's energy imbalance (EEI) (Hansen et al. 2005; Trenberth et al. 2014). Radiative forcing is a change in net radiant flux due to changes in external drivers of climate change, such as greenhouse gas

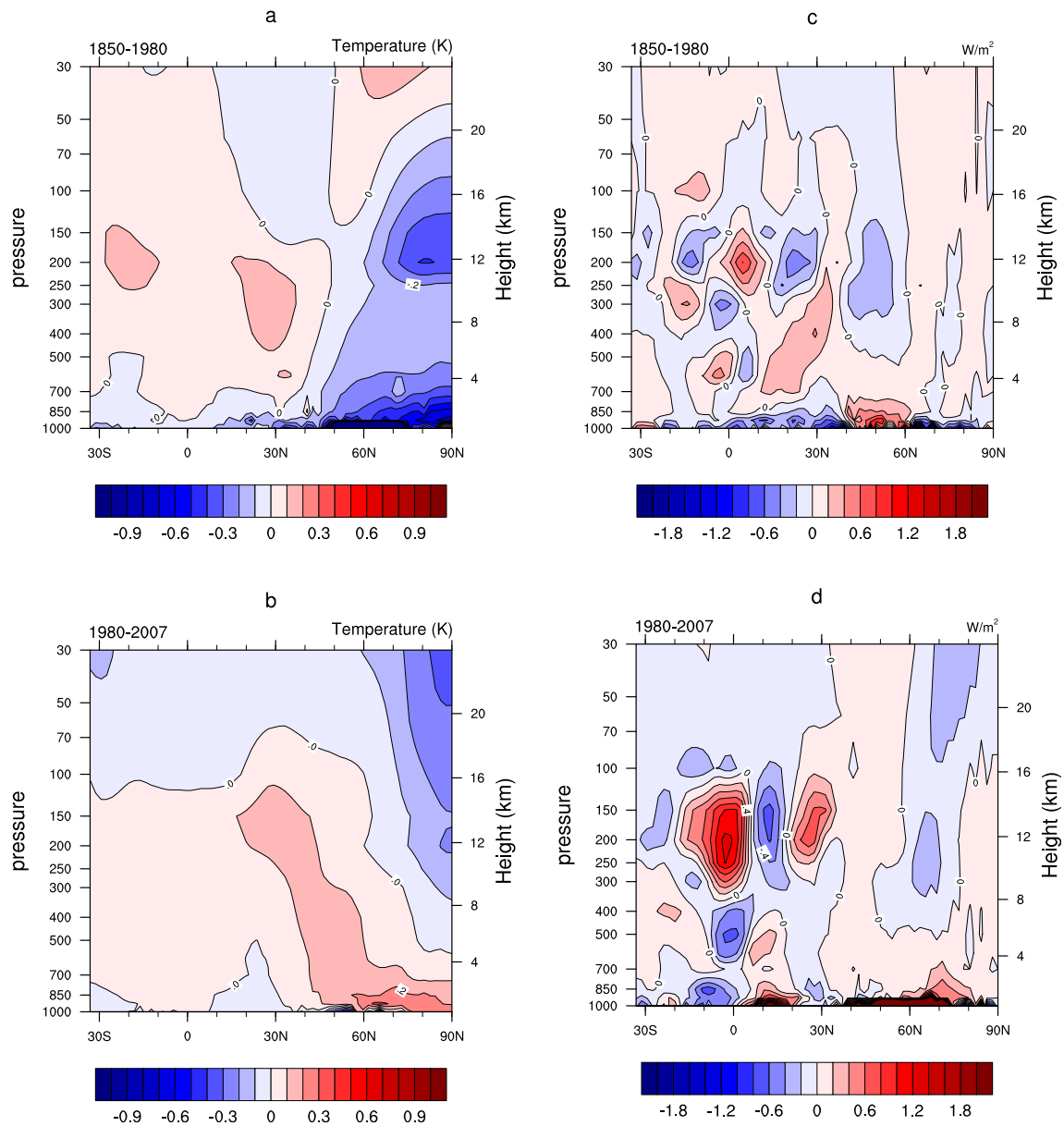


Fig. 7 Vertical change in atmospheric temperature (**a, b**) and meridional transport of heat (**c, d**), 1850–1980 (**a, c**), 1980–2007 (**b, d**)

concentrations and aerosol forcing. More than 90% of EEI is stored in ocean, increasing ocean heat content (OHC), which warms ocean (Cheng et al. 2017). Ocean circulation then transports heat to poles, causing sea ice melting. The exchange of heat between sea and air also warms atmosphere in the Arctic. In this experiment, the ocean does not participate in the global energy cycle. Energy is imbalanced in simulations with only atmospheric and land surface modules. The heat capacity of atmosphere is small and the ability to store energy is weak. Therefore, when the atmosphere gains extra energy, it quickly passes to colder regions of high latitudes. Arctic air temperature is mainly affected by colder ocean in the underlying surface, so that most significant area of warming in the Northern Hemisphere appears in the Siberian region.

4 Conclusions

We use Earth system models to simulate changes in global SIOAs emissions since the industrial revolution, and the response of surface temperatures in the Northern Hemisphere to changes in such pollutant emissions. With adjustment of global industrialization, there are two stages of SIOAs concentration changes in the Northern Hemisphere. From 1850 to 1980, SIOAs concentrations increase in the Northern Hemisphere, most notably in Europe and North America, which led to the temperature decreasing. During the year 1980 and 2007, SIOAs concentrations show an opposite trend in developed and developing regions of the Northern Hemisphere. There is a regional difference in temperature changes caused by this

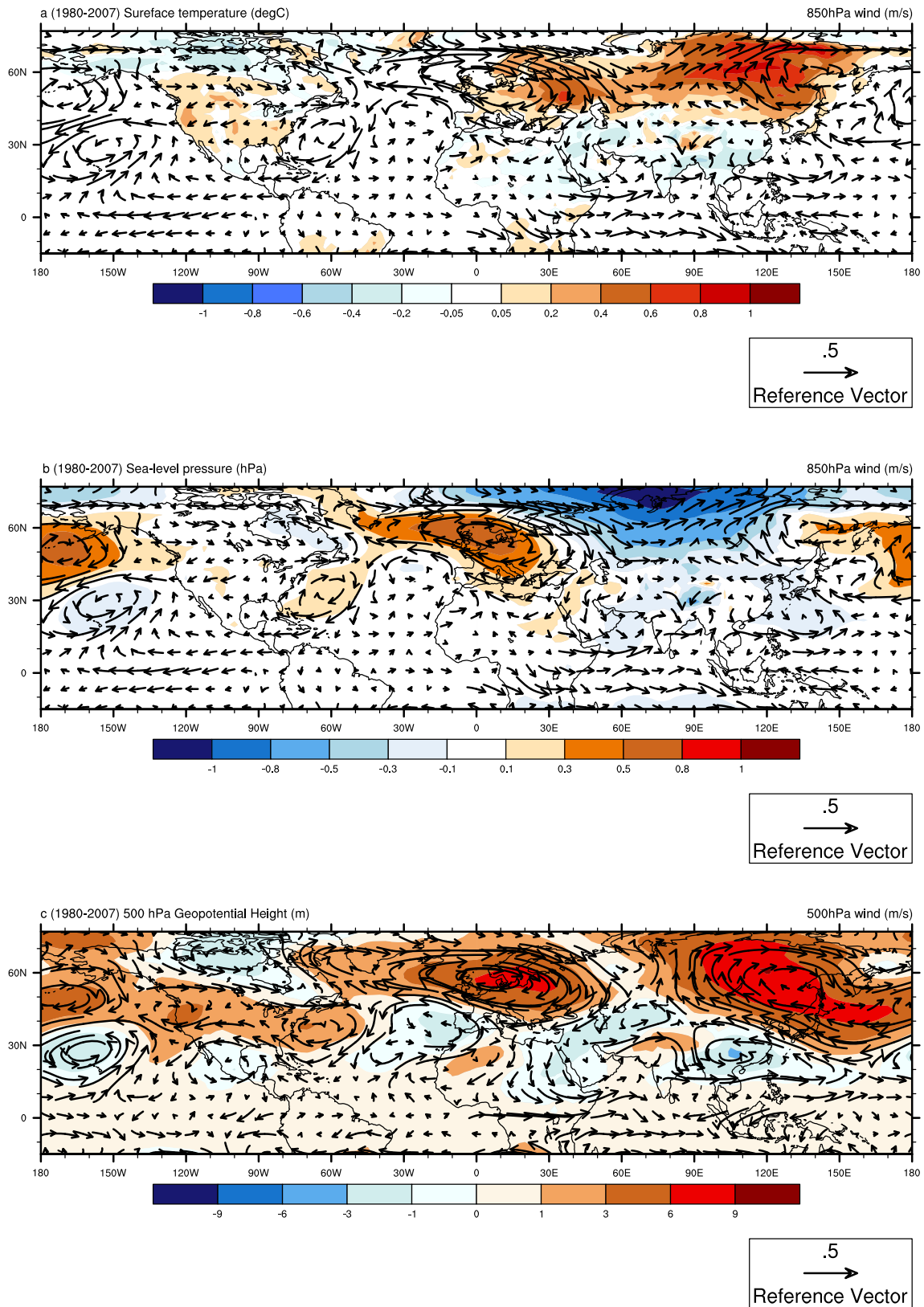


Fig. 8 From year 1980 to 2007. **a** 850 hPa wind field changes. The arrow in (a) is the 850 hPa wind field changes after the SIOA concentrations change. The color represents the change in average surface temperature. **b** Surface pressure changes. The arrow in (b) is the change in 850 hPa wind

field after SIOA concentrations change, and the color map shows the sea level pressure changes after SIOA concentration disturbance. **c** Change of 500 hPa geopotential height field (color map), vector arrow is change of 500 hPa wind field

difference in aerosol pollutant emissions. The main performance is temperature increasing in high latitudes of the Northern Hemisphere. Temperature reduces in mid-low latitudes of East Asia, in South Asia, and elsewhere.

The main cause of temperature change in source area is the effects of radiative forcing, such as Europe warming at first stage and cooling in East and South Asia during stage two. Long-distance response of temperature is mainly due to heat transfer. Although there is no obvious change in SIOAs concentrations in Eastern Siberia, the temperature response is significant.

Warm advection in the Siberian region is mainly due to adjustment of atmospheric circulation, which leads to the enhancement of southwesterly wind and southeasterly wind. This change in atmospheric circulation is due to the inability to store much energy by itself compared to ocean. So, it is necessary to quickly transfer additional solar radiation to other areas to maintain equilibrium. Ming et al. (2011) showed that aerosols increase baroclinic instability and enhance wind shear. Wilcox et al. (2019) find that the large-scale circulation response to Asian anthropogenic aerosol is primarily an extratropical-driven phenomenon, either through Rossby wave trains excited in the extratropics or through extratropical meridional temperature gradients. The differences between those conclusions due to differences in the local response to emissions. At the same time, the sensitivity of different models to aerosol emissions is very different. This adds additional complexity and complications in identifying the climate imprint of aerosols due to the large uncertainty in the atmospheric circulation response, especially at sub-continental scales.

This study only discusses the response to changes in global SIOAs emissions under the coupling of atmospheric and terrestrial modules. We only concern changes in radiant flux at the top of atmosphere and on the ground after changes in atmospheric composition, and adjustment of atmosphere in the event of energy imbalance. Ocean plays a non-negligible role in the storage and transport of radiant energy in the Earth system. So, we will add the ocean components to simulate temperature response to changes in aerosol emissions in future work.

Funding information This work was supported by the National Natural Science Foundation of China (41831175, 91937302 and 41721004). Key Deployment Project of Centre for Ocean Mega-Research of Science, Chinese academy of science(COMS2019QXX).

References

- Aas W, Mortier A, Bowersox V, Cherian R, Faluvegi G, Fagerli H, Hand J, Klimont Z, Galy-Lacaux C, Lehmann CMB et al (2019) Global and regional trends of atmospheric sulfur. *Sci Rep* 9:953. <https://doi.org/10.1038/s41598-018-37304-0>
- Acosta Navarro JC, Varma V, Riipinen I, Seland Ø, Kirkevåg A, Struthers H, Iversen T, Hansson HC, Ekman AML (2016) Amplification of Arctic warming by past air pollution reductions in Europe. *Nature Geoscience* 9:277–281. <https://doi.org/10.1038/ngeo2673>
- Bäumer D, Vogel B, Versick S, Rinke R, Möhler O, Schnaiter M (2008) Relationship of visibility, aerosol optical thickness and aerosol size distribution in an ageing air mass over South-West Germany. *Atmospheric Environment* 42:989–998. <https://doi.org/10.1016/j.atmosenv.2007.10.017>
- Bollasina MA, Ming Y, Ramaswamy V (2013) Earlier onset of the Indian monsoon in the late twentieth century: the role of anthropogenic aerosols. *Geophys. Res. Lett.* 40:3715–3720. <https://doi.org/10.1002/grl.50719>
- Boucher O, D. Randall (2013) Clouds and aerosols. *Climate change 2013: the physical science basis. Contribution of Working Group I to the Fifth Assessment Report of the Intergovernmental Panel on Climate Change chapter7*
- Cheng L, Trenberth KE, Fasullo J, Boyer T, Abraham J, Zhu J (2017) Improved estimates of ocean heat content from 1960 to 2015. *Science Advances* 3:e1601545. <https://doi.org/10.1126/sciadv.1601545>
- Conley AJ, Westervelt, D. M., Lamarque, J. F., Fiore, A. M., Shindell, D., Correa, G., Faluvegi, G., Horowitz, L. W. (2018) Multimodel surface temperature responses to removal of U.S. sulfur dioxide emissions. *Journal of Geophysical Research: Atmospheres* 123:2773–2796 <https://doi.org/10.1002/2017jd027411>
- Emmons LK, Walters S, Hess PG, Lamarque JF, Pfister GG, Fillmore D, Granier C, Guenther A, Kinnison D et al (2010) Description and evaluation of the Model for Ozone and Related chemical Tracers, version 4 (MOZART-4). *Geoscientific Model Development* 3:43–67. <https://doi.org/10.5194/gmd-3-43-2010>
- Gantt B, He J, Zhang X, Zhang Y, Nenes A (2014) Incorporation of advanced aerosol activation treatments into CESM/CAM5: model evaluation and impacts on aerosol indirect effects. *Atmospheric Chemistry and Physics* 14:7485–7497. <https://doi.org/10.5194/acp-14-7485-2014>
- Gates WL, Boyle JS, Covey C, Dease CG, Doutriaux CM, Drach RS, Fiorino M, Gleckler PJ et al (1999) An overview of the results of the Atmospheric Model Intercomparison Project (AMIP I). *Bulletin of the American Meteorological Society* 80:29–56. [https://doi.org/10.1175/1520-0477\(1999\)080<0029:aootro>2.0.co;2](https://doi.org/10.1175/1520-0477(1999)080<0029:aootro>2.0.co;2)
- Hansen J, Nazarenko L, Ruedy R, Sato M, Willis J, Genio D, Anthony K, Dorothy L, Andrew L, Ken MS, Novakov T, Perlwitz J, Russell G, Schmidt GA, Tausnev N (2005) Earth's energy imbalance: confirmation and implications. *Science* 308:1431–1435. <https://doi.org/10.1126/science.1110252>
- He J, Zhang Y, Glotfelty T, He R, Bennartz R, Rausch J, Sartelet K (2015) Decadal simulation and comprehensive evaluation of CESM/CAM5.1 with advanced chemistry, aerosol microphysics, and aerosol-cloud interactions. *Journal of Advances in Modeling Earth Systems* 7:110–141. <https://doi.org/10.1002/2014ms000360>
- Hoesly RM, Smith SJ, Feng L, Klimont Z, Janssens-Maenhout G, Pitkanen T, Seibert JJ, Vu L, Andres RJ, Bolt RM, Bond TC, Dawidowski L, Kholod N, Kurokawa J-i, Li M, Liu L, Lu Z, Moura MCP, O'Rourke PR, Zhang Q (2018) Historical (1750–2014) anthropogenic emissions of reactive gases and aerosols from the Community Emissions Data System (CEDS). *Geoscientific Model Development* 11:369–408. <https://doi.org/10.5194/gmd-11-369-2018>
- Kasoar M, Voulgarakis A, Lamarque JF, Shindell DT, Bellouin N, Collins WJ, Faluvegi G, Tsigaridis K (2016) Regional and global temperature response to anthropogenic SO₂ emissions from China in three climate models. *Atmospheric Chemistry and Physics* 16:9785–9804. <https://doi.org/10.5194/acp-16-9785-2016>

- Klimont Z, Smith SJ, Cofala J (2013) The last decade of global anthropogenic sulfur dioxide: 2000–2011 emissions. *Environmental Research Letters* 8. <https://doi.org/10.1088/1748-9326/8/1/014003>
- Knutti, R., D. Masson, and A. Gettelman (2013), Climate model genealogy: generation CMIP5 and how we got there, *grl*, 40, 1194–1199, <https://doi.org/10.1002/grl.50256>.
- Lamarque JF, Bond TC, Eyring V, Granier C, Heil A, Klimont Z, Lee D, Liousse C, Mieville A, Owen B et al (2010) Historical (1850–2000) gridded anthropogenic and biomass burning emissions of reactive gases and aerosols: methodology and application. *Atmospheric Chemistry and Physics* 10:7017–7039. <https://doi.org/10.5194/acp-10-7017-2010>
- Lamarque JF, Emmons LK, Hess PG, Kinnison DE, Tilmes S, Vitt F, Heald CL, Holland EA, Lauritzen PH, Neu J, Orlando JJ, Rasch P, Tyndall G (2011) CAM-chem: description and evaluation of interactive atmospheric chemistry in CESM. *Geoscientific Model Development Discussions* 4:2199–2278. <https://doi.org/10.5194/gmdd-4-2199-2011>
- Lamarque JF, Emmons LK, Hess PG, Kinnison DE, Tilmes S, Vitt F et al (2012) CAM-chem: description and evaluation of interactive atmospheric chemistry in the Community Earth System Model. *Geoscientific Model Development* 5:369–411. <https://doi.org/10.5194/gmd-5-369-2012>
- Lau WK-M, Kim K-M (2017) Competing influences of greenhouse warming and aerosols on Asian summer monsoon circulation and rainfall, Asia-Pacific. *Journal of the Atmospheric Sciences* 53(2): 181–194. <https://doi.org/10.1007/s13143-017-0033-4>
- Li X, Ting M, Li C, Henderson N (2015) Mechanisms of Asian summer monsoon changes in response to anthropogenic forcing in CMIP5 models. *Journal of Climate* 28(10):4107–4125. <https://doi.org/10.1175/JCLI-D-14-00559.1>
- Li X, Ting M, Lee DE (2018) Fast adjustments of the Asian summer monsoon to anthropogenic aerosols. *Geophysical Research Letters* 45:1001–1010. <https://doi.org/10.1002/2017GL076667>
- Lin J, Tong D, Davis S, Ni R, Tan X, Pan D, Zhao H, Lu Z, Streets D, Feng T, Zhang Q, Yan Y, Hu Y, Li J, Liu Z, Jiang X, Geng G, He K, Huang Y, Guan D (2016) Global climate forcing of aerosols embodied in international trade. *Nature Geoscience* 9:790–794. <https://doi.org/10.1038/ngeo2798>
- Liu X, Easter RC, Ghan SJ, Zaveri R, Rasch P, Shi X, Lamarque JF, Gettelman A, Morrison H, Vitt F, Conley A et al (2012) Toward a minimal representation of aerosols in climate models: description and evaluation in the Community Atmosphere Model CAM5. *Geoscientific Model Development* 5:709–739. <https://doi.org/10.5194/gmd-5-709-2012>
- Lu Z, Streets DG, Zhang Q, Wang S, Carmichael GR, Cheng YF, Wei C, Chin M, Diehl T, Tan Q (2010) Sulfur dioxide emissions in China and sulfur trends in East Asia since 2000. *Atmospheric Chemistry and Physics* 10:6311–6331. <https://doi.org/10.5194/acp-10-6311-2010>
- Ming Y, Ramaswamy V, Chen G (2011) A model investigation of aerosol-induced changes in boreal winter extratropical circulation. *J. Climate* 24:6077–6091. <https://doi.org/10.1175/2011JCLI4111.1>
- Myhre G, Shindell, D., Bréon, F.-M., Collins, W., Fuglestedt, J., Huang, J., et al. (2013) Anthropogenic and natural radiative forcing. In T F Stocker, et al (Eds), *Climate Change 2013: The Physical Science Basis Contribution of Working Group I to the Fifth Assessment Report of the Intergovernmental Panel on Climate Change*:650–740
- Neale RB, Chen, C. C., Gettelman, A., Lauritzen, P. H., Park, S., Williamson, D. L., et al. (2012) Description of the Community Atmosphere Model (CAM5) NCAR Tech Note NCAR/TN-486 + STR
- Ohara T, Akimoto H, Kurokawa J, Horii N, Yamaji K, Yan X, Hayasaka T (2007) An Asian emission inventory of anthropogenic emission sources for the period 1980–2020. *Atmospheric Chemistry and Physics Discussions* 7:6843–6902. <https://doi.org/10.5194/acpd-7-6843-2007>
- Oleson K, Dai, Y., Bonan, G. B., Bosilovich, M., Dickinson, R., Dirmeyer, P., ... Zeng, X. (2004) Technical Description of the Community Land Model (CLM) University Corporation for Atmospheric Research (No. NCAR/TN-461 + STR) <https://doi.org/10.5065/D6N877R0>
- Ramanathan V, Feng Y (2009) Air pollution, greenhouse gases and climate change: global and regional perspectives. *Atmospheric Environment* 43:37–50. <https://doi.org/10.1016/j.atmosenv.2008.09.063>
- Smith SJ, van Aardenne J, Klimont Z, Andres RJ, Volke A, Delgado Arias S (2011) Anthropogenic sulfur dioxide emissions: 1850–2005. *Atmospheric Chemistry and Physics* 11:1101–1116. <https://doi.org/10.5194/acp-11-1101-2011>
- Tilmes S, Lamarque JF, Emmons LK, Kinnison DE, Ma PL, Liu X, Ghan S, Bardeen C et al (2015) Description and evaluation of tropospheric chemistry and aerosols in the Community Earth System Model (CESM1.2). *Geoscientific Model Development* 8:1395–1426. <https://doi.org/10.5194/gmd-8-1395-2015>
- Trenberth KE, Fasullo JT, Balmaseda MA (2014) Earth's energy imbalance. *J Climate* 27:3129–3144. <https://doi.org/10.1175/jcli-d-13-00294.1>
- Tsigaridis K, Krol M, Dentener FJ, Balkanski Y, Lathière J, Metzger S, Hauglustaine DA, Kanakidou M (2006) Change in global aerosol composition since preindustrial times. *Atmospheric Chemistry and Physics Discussions* 6:5585–5628. <https://doi.org/10.5194/acpd-6-5585-2006>
- Undorf S, Bollasina M, Booth B, Hegerl (2018) Contrasting the effects of the 1850–1975 increase in sulphate aerosol in USA and WEU on Atlantic in CESM. *Geophysical Research Letters* 45:11,930–911, 940. <https://doi.org/10.1029/2018GL079970>
- Volkamer R, Jimenez JL, Martini S, Federico D, Katja Z, Qi S, Dara M, Luisa T, Worsnop DR, Molina MJ (2006) Secondary organic aerosol formation from anthropogenic air pollution: rapid and higher than expected. *Geophysical Research Letters* 33. <https://doi.org/10.1029/2006gl026899>
- Wang Y, Jiang JH, Su H (2015) Atmospheric responses to the redistribution of anthropogenic aerosols. *J. Geophys. Res. Atmos.* 120: 9625–9641. <https://doi.org/10.1002/2015JD023665>
- Wilcox LJ, Dunstone N, Lewinschal A, Bollasina M, Ekman AML, Highwood EJ (2019) Mechanisms for a remote response to Asian anthropogenic aerosol in boreal winter. *Atmos. Chem. Phys.* 19: 9081–9095. <https://doi.org/10.5194/acp-19-9081-2019>
- Xie S-P, Lu B, Xiang B (2013) Similar spatial patterns of climate responses to aerosol and greenhouse gas changes. *Nature Geoscience* 6(10):828–832. <https://doi.org/10.1038/ngeo1931>
- Xie X, Liu X, Wang H, Wang Z (2016) Effects of aerosols on radiative forcing and climate over East Asia with different SO₂ emissions. *Atmosphere-Basel* 7. <https://doi.org/10.3390/atmos7080099>

Publisher's note Springer Nature remains neutral with regard to jurisdictional claims in published maps and institutional affiliations.